(Received 17 November 2024, Accepted 18 December 2024, Scheduled 5 January 2025)

Two Compact Hybrid Band-Pass Filters Using Eighth-Mode Substrate-Integrated Waveguide and Microstrip Resonators

Luyao Tang[1, 2, *], Wei Han[1, 2], Hao Wei[1, 2], and Yanbin Li[1]

[1] *The 54th Research Institute of China Electronics Technology Group Corporation, China*
[2] *National Engineering Reasearch Center of Communication Software and Asic Design, China*

ABSTRACT: Two compact substrate-integrated waveguide (SIW) filters with hybrid coupling of eighth-mode substrate integrated waveguide (EMSIW) resonators and microstrip are proposed in this paper. Hybrid coupled filters were achieved by etching two half-wavelength microstrip resonators (BPF I) or two quarter-wavelength microstrip resonators (BPF II) on the top of traditional second-order EMSIW filters. The topology of the two filters was analyzed. Due to the cross coupling between resonator 1 and resonator 4, two transmission zeros were achieved outside the band of BPF I, which increased the selectivity of the filter. Due to the mixed electromagnetic coupling between resonator 2 and resonator 3, a transmission zero is realized in the stopband of BPF II. To confirm the validity of the two filter models, two filters were designed, produced, and measured. Based on the findings of the measurements, the central frequency of BPF I is recorded at 7.7 GHz, with a fractional bandwidth (FBW) of 18.2%. The insertion loss (IL) within the passband is minimal at 0.8 dB, and the size of the filter is only 8 mm $*$ 4 mm ($0.53\lambda_g * 0.26\lambda_g$). The filter exhibits enhanced out-of-band suppression due to the presence of two transmission zeros located at frequencies of 6.4 GHz and 10 GHz. The center frequency of BPF II is 19.5 GHz,; the FBW is 20.5%; the IL within the passband is only 0.49 dB; and the size of the filter is only 2 mm $*$ 2 mm ($0.34\lambda_g * 0.34\lambda_g$). As a result of the mixed electromagnetic coupling effects, a transmission zero occurs at a frequency of 26.7 GHz. The simulation outcomes are consistent with the experimental findings. Compared with other reported SIW filters, the two filters introduced in this study exhibit favorable characteristics such as reduced insertion loss and compact dimensions.

1. INTRODUCTION

Substrate integrated waveguides are frequently employed in the development of high-performance filters due to their favorable characteristics, including reduced loss, elevated quality factor, and straightforward integration [1–3]. However, compared to filters with microstrip resonators, SIW filters have no advantage in size. In recent years, with the advancement of system integration technology, communication systems have become increasingly compact [4, 5]. The large size of SIW filters has hindered their widespread application. Therefore, there is a need for research focused on miniaturizing SIW filters.

The multi-layer SIW filter based on processes such as microelectromechanical system (MEMS) and low-temperature co-fired ceramics (LTCC) is an effective method for miniaturization. This method achieves smaller dimensions by increasing the number of metal conductor layers. In [6], a compact SIW filter utilizing LTCC technology was suggested. The filter achieves a small size by stacking six cavities on a three-layer substrate. The volume of the filter is $7 * 3.8 * 1.2\,\text{mm}^3$ ($0.65\lambda_0 * 0.35\lambda_0 * 0.11\lambda_0$), which is smaller than single-layer SIW filters. In [7], a folded ridge integrated waveguide (FRSIW) was proposed based on the multi-layer printed circuit board (PCB) process by folding the traditional ridge integrated waveguide (RSIW). The size of the filter is $0.35\lambda_g * 2.41\lambda_g$, Where λ_g is the guided wavelength in the dielectric substrate. In [8], a compact SIW filter is proposed by folding a quarter-mode SIW cavity using MEMS technology. The filter's fractional bandwidth is 9%, with an IL of 2.7 dB, and dimensions measuring $0.736\lambda_g * 0.736\lambda_g * 0.028\lambda_g$. In [9], a miniaturized ridge SIW filter using a two-layer substrate was proposed. This specific design leads to a decrease in size by 62% in comparison to the conventional SIW filter. Although multi-layer SIW based on multi-layer technology can significantly reduce the size of filters, it is not suitable for single-layer substrates.

Utilizing SIW non-holonomic mode resonators proves to be a successful approach in facilitating the miniaturization of SIW filters. The electromagnetic field distribution characteristics of SIW remain consistent when the SIW is bisected along its symmetrical plane, owing to the symmetrical nature of the electromagnetic field distribution within the SIW structure. Based on this principle, half-mode substrate integrated waveguide (HMSIW), quarter-mode substrate integrated waveguide (QMSIW), and EMSIW were proposed and used in the design of filters [10–12]. In [13], two miniaturized filters were proposed using QMSIW and EMSIW. In [14], a compact filter based on EMSIW resonator was proposed, featuring an IL of 2.53 dB and physical dimensions of $0.55\lambda_g * 0.65\lambda_g$. In [15], a compact SIW filter utilizing HMSIW was proposed, with an IL of 1.57 dB and a size of $0.84\lambda_g * 0.45\lambda_g$. In [16], a fourth-order SIW filter was developed using QMSIW. To decrease the insertion loss of the filter, a shielding configuration was incorporated surrounding the QMSIW resonator. The filter exhibits an IL of 0.63 dB,

* Corresponding author: Luyao Tang (tangluyao613@163.com).

with dimensions $0.76\lambda_0 * 0.43\lambda_0$. The size of SIW filters using non-holonomic modes is smaller than traditional SIW filters, but filters employing non-holonomic mode SIW resonators often exhibit higher insertion loss.

Loading structures or materials that modify the distribution of electromagnetic fields on SIW resonators is also an effective method for miniaturizing SIW filters. In [17], a miniaturized filter was achieved by loading four complementary split-ring resonators (CSRRs) on SIW, with an IL of 1.96 dB and a size of $0.756\lambda_g * 0.57\lambda_g$. In [18], a compact SIW filter with dimensions of $0.31\lambda_g * 1.18\lambda_g$ was designed by periodically etching distinctive electromagnetic bandgap elements on the SIW. In [19], the isolation of electric and magnetic fields was accomplished by incorporating metalized through holes within the substrate of the SIW to induce a slow-wave phenomenon, leading to a 40% decrease in the longitudinal dimension of the SIW. In [20], a filter was designed by combining the SIW and defected ground structures (DGS). The IL of the filter is measured at 0.8 dB, with the dimensions of the filter being $0.57\lambda_g * 1.07\lambda_g$.

The use of dual-mode or multi-mode resonant structures can achieve the miniaturization of filters. In [21], a third-order SIW filter with metal hole perturbation is proposed. This design incorporates perturbations in the form of metal holes at the center of the SIW, which results in the adjustment of the resonator's fundamental mode towards the secondary mode, thereby generating the passband for the filter. The IL of the filter is 2.2 dB, and the filter size is $0.72\lambda_0 * 0.72\lambda_0$. In [22], a low-loss Ka-band LTCC filter based on a multimode SIW resonator was proposed. Four mode couplings were formed inside the cavity through perturbations through metal via holes. The IL of the filter is 0.8 dB, while the size is only $0.64\lambda_g^2$. In [23], a compact dual-band SIW filter was proposed using a perturbation structure. In [24], Multimode resonance is attained through the incorporation of a set of through-hole disturbances and two variations of slotted lines to regulate the convergence of modes. A compact dual-band SIW filter was proposed utilizing a multi-mode resonator. The utilization of dual-mode/multimode technology often involves coupling multiple resonant modes within a single resonator, thereby reducing the number of resonators and achieving miniaturization. However, dual-mode/multi-mode resonant perturbation techniques typically shift the fundamental mode frequency close to the secondary mode, which diminishes the miniaturization effect of this method.

Recently, hybrid coupling structures combining SIW and planar microstrip structures have been used to achieve miniaturization of SIW filters [25, 26]. In [27], A fourth-order SIW filter was developed by employing a hybrid configuration that combines SIW with microstrip resonators. Cross coupling was introduced using microstrip resonators, and two transmission zeros were introduced outside the band, which improved the selectivity of the filter. The filter exhibits an IL of 1.42 dB and has physical dimensions of $0.9\lambda_0 * 0.56\lambda_0$. In [28], a compact third-order filter structure combining SIW and stripline was proposed. The stripline resonator is positioned within two substrate integrated waveguide cavities, enabling an increase in the filter's order without necessitating additional physical dimensions. In contrast to the conventional third-order SIW filter, the dimensions of this filter have been decreased by 33%.

Numerous techniques for reducing the size of SIW filters have been suggested; however, the dimensions of SIW filters continue to be relatively larger in comparison to microstrip filters. The development of SIW filters that are both compact in size and have minimal insertion loss continues to present notable difficulties. In response to the miniaturization problem of SIW filters, this paper proposes two novel compact hybrid SIW filter structures combining EMSIW and microstrip resonators. Two microstrip resonators are embedded in two EMSIWs, achieving fourth-order resonator hybrid coupling without requiring additional space. These structures exhibit low insertion loss, wide bandwidth, high selectivity, and compact size.

The subsequent sections of this article are structured in the following manner. In the second section, two fourth-order hybrid filters are designed. These filters are composed of half-wavelength microstrip resonators or quarter-wavelength microstrip resonators combined with two EMSIWs. In the third section, two compact filters are manufactured, measured, and compared with other miniaturized SIW filters, demonstrating the advantages of the filter structure proposed in this paper. Ultimately, the fourth section of the document provides the conclusion.

2. FILTER DESIGN AND ANALYSIS

The two compact SIW filters in this article are both realized on a single-layer alumina substrate with a thickness of 0.254 mm and a relative dielectric constant of 9.9. These filters consist of two EMSIW resonators and two half-wavelength microstrip resonators or two quarter-wavelength microstrip resonators. In contrast to the resonant cavity based on SIW, the resonant cavity utilizing EMSIW technology has undergone a reduction in size by 87.5%. Figure 1 illustrates the electric field distribution in the conventional SIW, HMSIW, QMSIW, and EMSIW cavities resonating under the main mode TE_{101}.

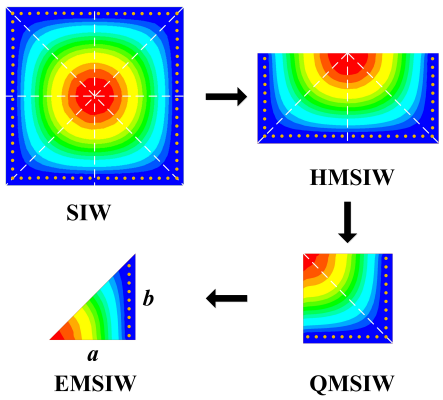

FIGURE 1. Electric field distribution of SIW, HMSIW, QMSIW, and EMSIW.

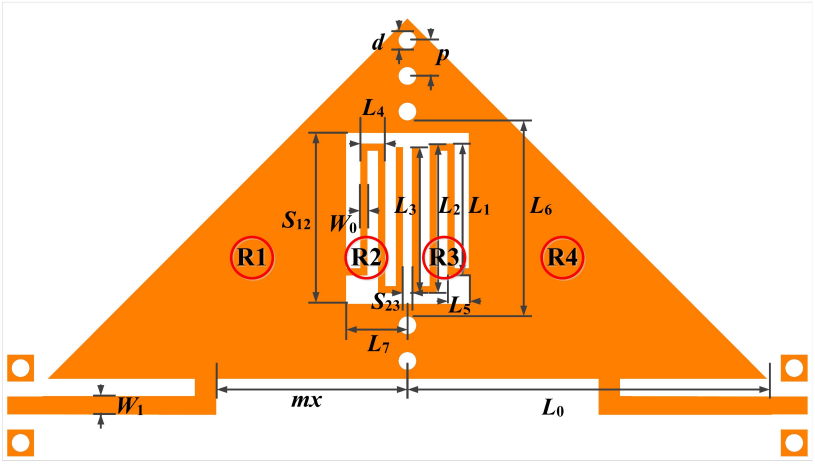

FIGURE 2. The structure of the filter based on EMSIW and half-wavelength microstrip resonators (BPF I).

The resonant frequency of the EMSIW cavity can be estimated by the following equation [29]:

$$f_{TE101} = \frac{c}{2\pi\sqrt{\mu_r\varepsilon_r}}\sqrt{\left(\frac{\pi}{a_{eff}}\right)^2+\left(\frac{\pi}{b_{eff}}\right)^2} \quad (1)$$

$$a = a_{eff}+\frac{d^2}{0.95p}-\Delta\omega \quad (2)$$

$$b = b_{eff}+\frac{d^2}{0.95p}-\Delta\omega \quad (3)$$

$$\frac{\Delta\omega}{h} = \left(0.05+\frac{0.3}{\varepsilon_r}\right)\times\ln\left(0.79\frac{(a_{eff}/2)^2}{h^3}+\frac{104(a_{eff}/2)-261}{h^2}+\frac{38}{h}+2.77\right) \quad (4)$$

where $f_{TE_{101}}$ is the resonant frequency of TE_{101} mode, and c represents the speed of light in vacuum. μ_r and ε_r are the relative magnetic permeability and relative dielectric constant of the substrate. a_{eff} and b_{eff} represent the edge lengths of the equivalent resonant cavity. a and b represent the initial dimensions of the EMSIW, while h represents the thickness of the substrate. d and p refer to the diameter of the metalized through-hole and the distance between the centers of adjacent through-holes, while $\Delta\omega$ represents the impact of the equivalent magnetic wall edge field.

2.1. BPF Using EMSIW and Half-Wavelength Microstrip Resonators (BPF I)

Figure 2 illustrates the configuration of the suggested SIW filter, which is constructed using EMSIW and half-wavelength microstrip resonators. It consists of two EMSIW resonators and two half wavelength microstrip resonators embedded within the EMSIW. L_0 in the structural parameters of the EMSIW resonator is equal to half of parameter a as described in Equation (2), while h represents the thickness of the substrate. This filter achieves the coupling of four resonators and has only the size of a second-order EMSIW filter, which is 50% smaller than the size of a conventional fourth-order EMSIW resonator. The filter is connected to the source and load through tap feeding. For testing convenience, the microstrip tap is converted to a Ground Signal Ground (GSG) tap. R1, R2, R3, R4 represent the four resonators that make up the filter, where R1 and R4 are EMSIW resonators, and R2 and R3 are microstrip resonators. The filter topology provides two signal transmission paths: path one goes from R1 to R2 to R3 and then to R4, while path two goes directly from R1 to R4. The two transmission paths above achieve cross-coupling, offering the potential to introduce finite transmission zeros outside the band.

R1 and R2 are coupled through direct contact, while the coupling between R2 and R3 consists of parallel microstrip lines. Simulate and analyze the electromagnetic coupling between four resonators using high frequency simulator software. Figure 3(a) illustrates the magnetic field distribution coupling between R1 and R2. The magnetic field at the connection between the EMSIW resonator and the microstrip resonator is strong, the main coupling between R1 and R2 is magnetic coupling. The coupling strength between R1 and R2 is related to parameter S_{12}. Figure 3(b) shows the coupled electric field distribution between R2 and R3, where energy transfer between the two microstrip resonators is mainly achieved through electrical coupling. The coupling strength between R2 and R3 is determined by the spacing S_{23} between the resonators. The coupling between R1 and R4 is primarily magnetic, and the magnitude of the coupling coefficient between R1 and R4 is influenced by the inductance of L_6.

The topology of the SIW filter based on EMSIW and half-wavelength microstrip resonators is shown in Figure 4. S/L represents the source and load of the filter, while Q_e is the external Q factor used to characterize the coupling between S/L and R1/R4. The value of Q_e is related to the position of the tap. k_{ij} represents the coupling strength between resonator i and resonator j. The center frequency of the hybrid structure EMSIW band-pass filter proposed in this paper is 7.7 GHz, with a FBW

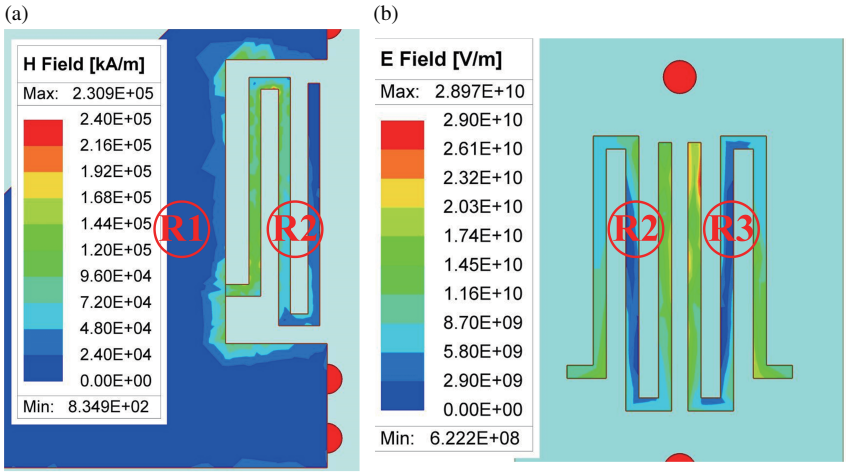

FIGURE 3. Electromagnetic field distribution between resonators. (a) Magnetic field distribution between R1 and R2. (b) Electric field distribution between R2 and R3.

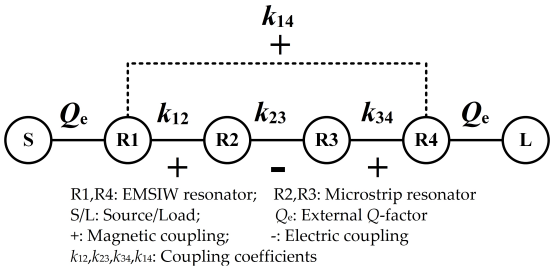

FIGURE 4. The topology of the filter based on EMSIW and half-wavelength microstrip resonators.

of 18.2%. According to the coupling matrix extraction method [30], the external Q factor can be extracted as $Q_e = 4.43$. The coupling matrix M can be formulated as represented in Equation (5).

$$M = \begin{bmatrix} 0 & 0.996 & 0 & 0 \\ 0.996 & 0 & 0.747 & 0 \\ 0 & 0.747 & 0 & 0.996 \\ 0 & 0 & 0.996 & 0 \end{bmatrix} \tag{5}$$

The coupling coefficients (k_{12}, k_{23}) can be calculated from entries of M:

$$k_{12} = m_{12} \cdot FBW \tag{6}$$

$$k_{23} = m_{23} \cdot FBW \tag{7}$$

Combining Equations (6)–(7) with the FBW of the filter to be designed, $k_{12} = 0.181$ and $k_{23} = 0.136$ can be obtained. According to formulas (1)–(4), the structural parameters of R1 can be preliminarily determined. Subsequently, the Eigenmode simulation in High frequency simulation software can be used to fine-tune the structural parameters of R1 to achieve a resonant frequency of 7.7 GHz. The structural characteristics of R2 may be ascertained by considering the central frequency and substrate properties. The electric field distribution of R1 and R2 is shown in Figure 5.

The coupling coefficient between EMSIW resonator and half-wavelength microstrip resonator, and the coupling coefficient between half-wavelength microstrip resonators are calculated using formula (6)–(7). The variable k_{12} denotes the coupling coefficient between R1 and R2, dependent on the parameter S_{12}. Similarly, k_{23} signifies the coupling coefficient between R2 and R3, determined by the parameter S_{23}. The diagram illustrating the interconnection between resonators is presented in Figure 6.

The coupling coefficient can be determined by utilizing Equation (8).

$$k = \frac{f_2^2 - f_1^2}{f_2^2 + f_1^2} \tag{8}$$

where f_1 and f_2 respectively represent the coupling frequency between two coupled resonators. The relationship between f_1 and f_2 is determined by the following equation:

$$f_0 = \sqrt{f_1 * f_2} \tag{9}$$

Figure 7 and Figure 8 show the coupling coefficients k_{12} and k_{23}. According to the coupling coefficient curve, as the parameter S_{12} increases, the coupling coefficient k_{12} increases, while the coupling coefficient k_{23} decreases with the increase of the coupling distance S_{23}. The coupling coefficients $k_{12} = 0.181$ and $k_{23} = 0.136$ can be derived from the coupling matrix. Comparing the coupling coefficient with the coupling curves in Figure 7 and Figure 8, the structural parameters of the filter were determined as $S_{12} = 1.92$ mm and $S_{23} = 0.1$ mm. The external Q factor is used to characterize the coupling relationship between the source/load and R1/R4. The external Q factor of the filter is influenced by the placement of the input and output taps, while the Q_e of the filter is related to the parameter mx. The external Q factor of the filter can be obtained using formula (10).

$$Q_e = \frac{\tau_{S_{11}}(f_0)\pi f_0}{2} \tag{10}$$

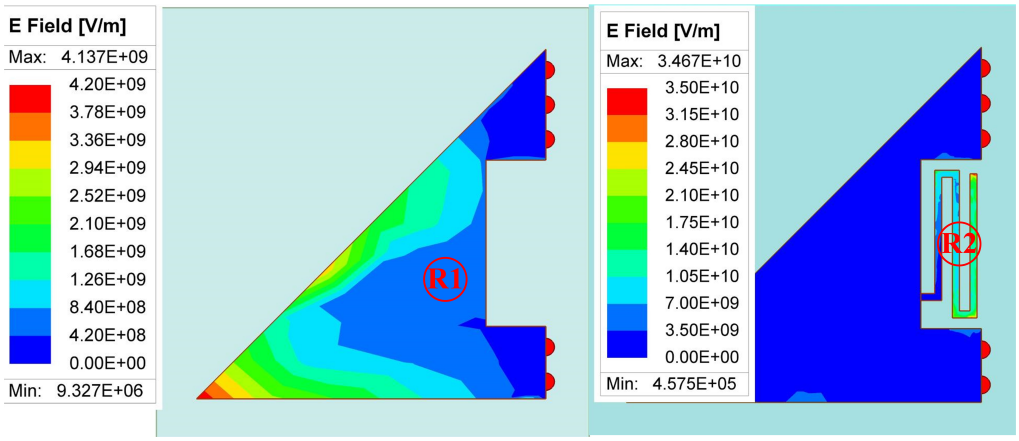

FIGURE 5. Simulation of electric field distribution in EMSIW resonator and half-wavelength microstrip resonator.

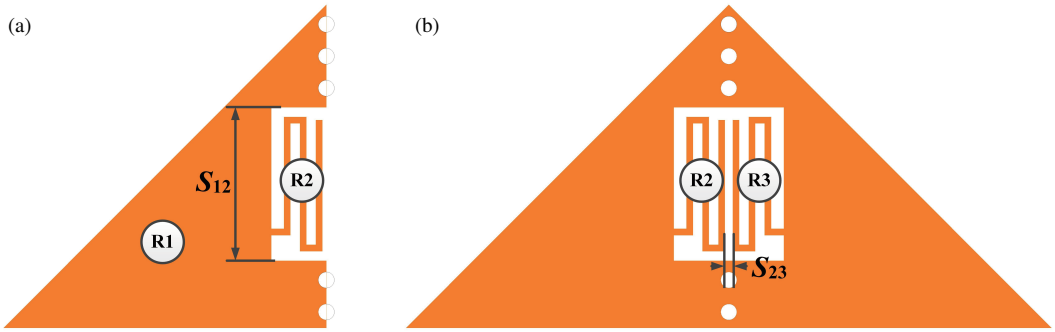

FIGURE 6. Coupling between resonators. (a) Coupling between EMSIW and half wavelength microstrip resonators. (b) Coupling between half wavelength microstrip resonators.

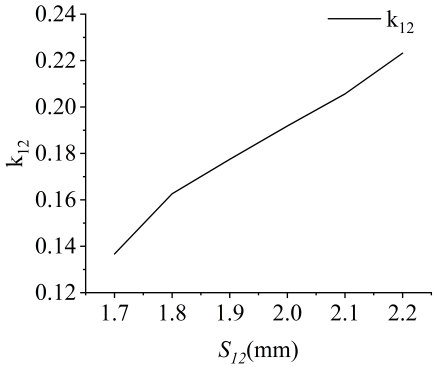

FIGURE 7. The coupling coefficient k_{12}.

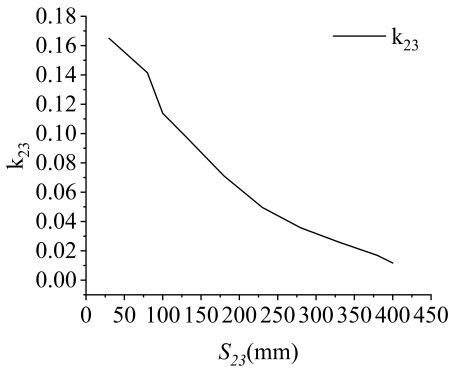

FIGURE 8. The coupling coefficient k_{23}.

The relationship curve between the external Q factor and mx is shown in Figure 9. Combined with the $Q_e = 4.43$ of the filter, the parameter $mx = 2.2$ can be obtained.

All structural parameters of the filter were obtained using the methods described above. Considering parasitic effects, the designed filter was fine tuned to obtain the structural parameters of the filter, as shown in Table 1. According to the simulation results, the center frequency of the filter is 7.7 GHz, the FBW is 18.2%, and the minimum in band IL is 0.57 dB. As a result of the cross-coupling, there are two transmission zeros at 6.3 GHz and 10 GHz outside the filter band. The attenuation levels for out-of-band signals are measured at -28.4 dB at 6.3 GHz and -48.6 dB at 10 GHz.

2.2. BPF Using EMSIW and Quarter Wavelength Microstrip Resonators (BPF II)

The structure of BPF II is shown in Figure 10. It consists of two EMSIW resonators and two quarter-wavelength microstrip resonators. This filter is comprised of two additional quarter-

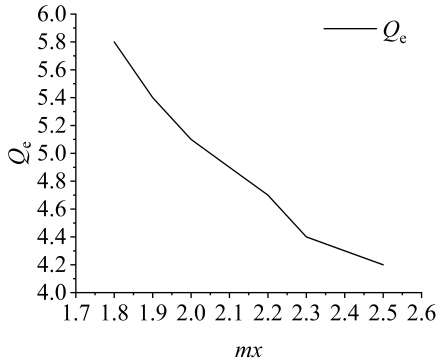

FIGURE 9. External Q-factor simulation of filters.

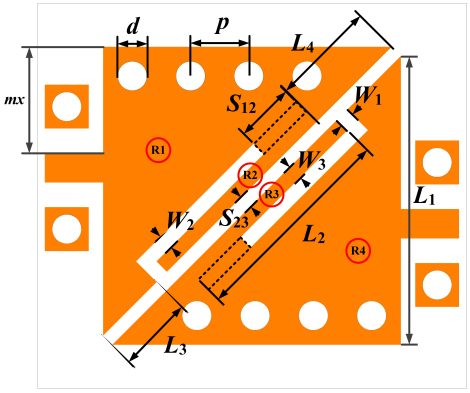

FIGURE 10. SIW filter structure based on EMSIW and quarter-wavelength microstrip resonators (BPF II).

TABLE 1. Dimensions of BPF I (unit: mm).

W_0	W_1	L_0	L_1	L_2	L_3	L_4
0.08	0.21	4	1.4	1.68	1.64	0.28
L_5	L_6	S_{12}	S_{23}	mx	L_7	
0.24	2.2	1.92	0.1	2.2	0.69	

wavelength microstrip resonators etched onto a second-order electrically coupled EMSIW filter to create a fourth-order resonator coupling. The two etched microstrip resonators can enhance the bandwidth and suppression of the filter without increasing its size. The filter uses a GSG form tap for feeding.

The topology of BPF II is shown in Figure 11. R1 and R3 in the topology represent two EMSIW resonators, while R2 and R3 represent two quarter-wavelength microstrip resonators. The two microstrip resonators in the EMSIW resonator are coupled through the end of the quarter-wavelength resonator, and the coupling strength varies with S_{12}. Two quarter-wavelength microstrip resonators are coupled through parallel microstrip lines, and the coupling strength between the two quarter-wavelength microstrip resonators is related to the spacing S_{23}.

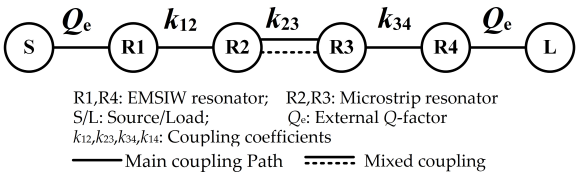

FIGURE 11. The topology of BPF II based on EMSIW and quarter-wavelength microstrip resonators.

The desired center frequency for the BPF II under design is 19.5 GHz, accompanied by a bandwidth of 4 GHz. By combining the center frequency $f_0 = 19.5$, the structural dimensions of each resonator can be preliminarily obtained through formulas (1)–(4).

Using the same design process as BPF I, the coupling coefficients between resonators are extracted through eigenmode simulation. The correlation between R1 and R2 is denoted by the coupling coefficient k_{12}, which is associated with the scattering parameter S_{12}. The coupling coefficient between R2 and R3 is represented by k_{23}, which is related to S_{23}. The coupling coefficient between resonators is shown in Figure 12. The external Q factor of the filter is related to the tap position. Figure 13 shows the curve depicting the relationship between the external Q factor and the parameter mx.

The center frequency of BPF II is 19.5 GHz, with a bandwidth of 4 GHz. The coupling matrix M can be formulated as represented in Equation 11. According to formulas (1)–(4), $k_{12} = k_{34} = 0.225$, $k_{23} = 0.168$ and $Q_e = 3.57$. By comparing the coupling coefficient curve with the external Q factor curve, the structural dimensions of BPF II can be obtained as shown in Table 2.

$$M = \begin{bmatrix} 0 & 0.996 & 0 & 0 \\ 0.996 & 0 & 0.747 & 0 \\ 0 & 0.747 & 0 & 0.996 \\ 0 & 0 & 0.996 & 0 \end{bmatrix} \tag{11}$$

TABLE 2. Dimensions of BPF II (unit: mm).

W_1	W_2	W_3	L_1	L_2	L_3
0.1	0.1	0.1	2	1.42	0.46
L_4	mx	S_{12}	S_{23}	d	p
0.7	0.8	0.39	0.09	0.2	0.4

According to the simulation results, the filter's central frequency is 19.5 GHz, with a bandwidth of 4 GHz and a minimum IL of 0.22 dB within the band. Due to the mixed electromagnetic coupling between R2 and R3 [31], there is a transmission zero at 26.6 GHz outside the filter band. The out-of-band suppression system at 26.6 GHz is -53.8 dB.

3. EXPERIMENT AND VERIFICATION

To validate the proposed filter structures, two hybrid coupled EMSIW filters were fabricated using thin film technology. Figure 14(a) shows a prototype photo of a filter coupled with EMSIW and half-wavelength microstrip resonators. The size of BPF I is $8\,\text{mm} * 4\,\text{mm}$ ($0.53\lambda_g * 0.26\lambda_g$). Figure 14(b)

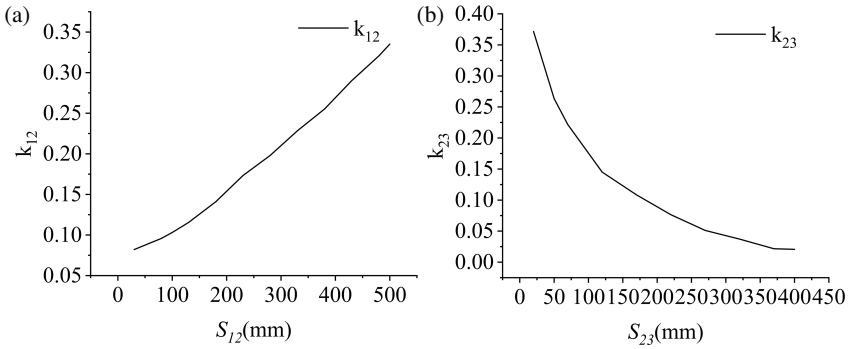

FIGURE 12. Coupling coefficient extraction. (a) Extracted coupling coefficient k_{12} for S_{12}. (b) Extracted coupling coefficient k_{23} for S_{23}.

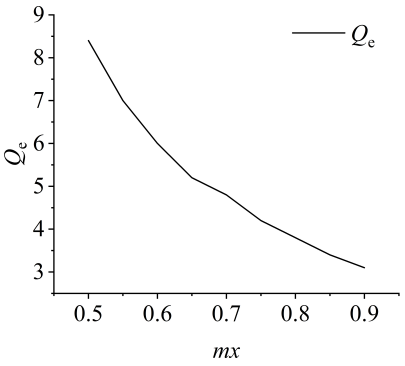

FIGURE 13. Extraction results of external Q factors.

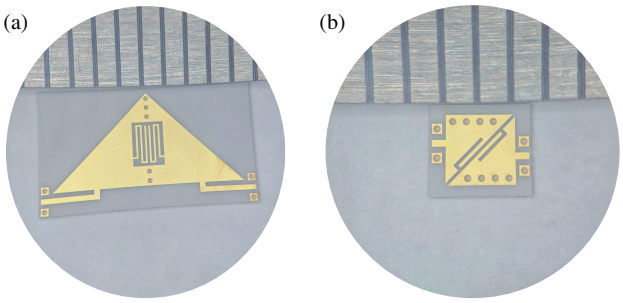

FIGURE 14. Prototype photo of filters. (a) Photo of BPF I. (b) Photo of BPF II.

shows a prototype photo of a filter coupled with EMSIW and quarter-wavelength microstrip resonators. The size of BPF II is $2\,\text{mm} * 2\,\text{mm}$ ($0.34\lambda_g * 0.34\lambda_g$). The probe station and vector network analyzer were utilized for the measurement of the two filters that were suggested. The measurement photos of the two filters proposed in this article are shown in the Figure 15.

The comparison of EM simulation and measurement results of EMSIW mixed coupling with half-wavelength microstrip resonators is shown in Figure 16. The passband of this filter is 7 GHz–8.4 GHz, with a FBW of 18.2%. The minimum IL in the band is 0.8 dB. Two transmission zeros were achieved at 6.4 GHz and 10 GHz, with an out-of-band rejection of -24.6 dB at 6.4 GHz and 46.6 dB at 10 GHz.

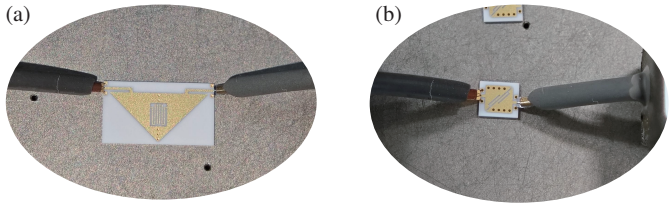

FIGURE 15. Filters measurement. (a) Measurement photo of BPF I. (b) Measurement photo of BPF II.

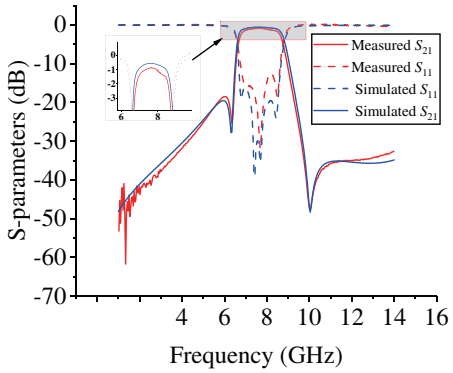

FIGURE 16. Comparison between Simulation and Measurement Results of BPF I.

The comparison of EM simulation and measurement results of mixed coupling between EMSIW and quarter-wavelength microstrip resonators is shown in Figure 17. The passband of this filter is 17.5 GHz–21.5 GHz, with a FBW of 20.5%. The minimum IL in the band is 0.49 dB. A transmission zero point has been achieved at 26.7 GHz, and the suppression at 26.7 GHz is -43.8 dB. The correlation between the measured S_{21} parameters and the simulation outcomes is satisfactory. However, the measured in-band return loss has shown a decline relative to the simulated values. The two filters discussed in this study are fabricated utilizing thin film technology. This technology offers a processing accuracy of ± 2 µm for graphical elements, with minimal impact on filter performance. Conversely, the accuracy of hole positioning in the thin film process is ± 30 µm, indicating that any positional deviations of the metal through-holes within the filter can adversely affect its in-band return loss. A simulation was conducted to assess the effects of vary-

TABLE 3. Comparison with other SIW filters.

Ref.	f_0	FBW	IL (dB)	Order	Number of TZs	Size	Technology
[13]	7.95	21.4%	1.59	3	1	$0.73\lambda_g * 0.74\lambda_g$	QMSIW + Microstrip
[15]	10.71	10%	1.57	3	2	$1.25\lambda_g * 0.67\lambda_g$	HMSIW + Microstrip
[17]	22.95	11.76%	1.96	4	2	$0.76\lambda_g * 0.57\lambda_g$	SIW + CSRR
[20]	6.18	8.1%	0.8	3	0	$1.06\lambda_g * 0.56\lambda_g$	SIW + DGS
[27]	11.51	6.78%	1.42	4	2	$1.33\lambda_g * 0.83\lambda_g$	SIW + Microstrip
[28]	9.96	7.43%	1.52	4	2	$1.38\lambda_g * 0.69\lambda_g$	SIW + Stripline
[32]	102.07	3.5%	1.58	5	1	$2.18\lambda_g * 1.54\lambda_g$	SIW + TSV
[33]	10	11.3%	0.9	3	1	$0.65\lambda_g * 0.95\lambda_g$	SIW + Stripline
[34]	9.99	10.9%	0.87	4	2	$1.18\lambda_g * 0.57\lambda_g$	SIW + Microstrip
BPF I	7.7	18.2%	0.8	4	2	$0.53\lambda_g * 0.26\lambda_g$	SIW + Microstrip
BPF II	19.5	20.5%	0.49	4	1	$0.34\lambda_g * 0.34\lambda_g$	SIW + Microstrip

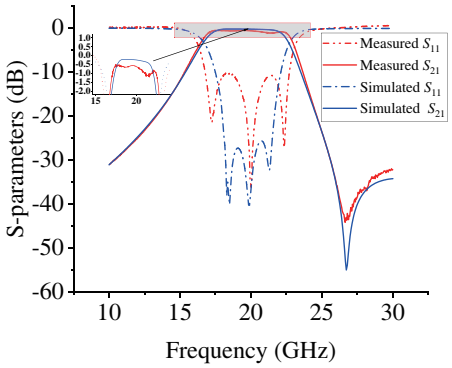

FIGURE 17. Comparison between Simulation and Measurement Results of BPF II.

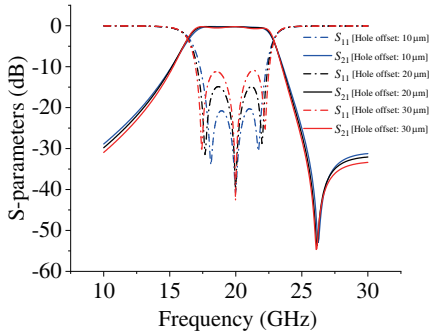

FIGURE 18. The impact of hole position inaccuracies on the filter.

ing through-hole offsets on filter performance, with the results illustrated in Figure 18. The findings indicate that as the offset of the hole position increases, the in-band return loss of the filter deteriorates.

Table 3 provides a comparative analysis of the two compact EMSIW hybrid coupled filters introduced in this study with previously reported SIW filters. The results indicate that the hybrid coupled SIW filters proposed in this article have lower insertion loss and smaller size.

4. CONCLUSIONS

This article presents two compact SIW BPFs with hybrid coupling of EMSIW resonators and microstrip resonators. In contrast to conventional SIW resonators, EMSIW resonators offer the benefit of reduced size. The method of etching microstrip resonators on EMSIW resonators increases the order of the filter without increasing its size, which is advantageous for filter miniaturization. In addition, there is cross coupling or mixed electromagnetic coupling between the filters, which results in transmission zeros out of the band, enhancing the selectivity of the filters. The two SIW filters that were proposed demonstrate favorable characteristics of minimal insertion loss and compact dimensions, rendering them well-suited for integration within RF microsystems utilized in satellite communication, as evidenced by experimental and measurements.

REFERENCES

[1] Li, D., W. Luo, X. Chen, J. Wang, C. Yang, K.-D. Xu, and Q. Chen, "SIW cavity mode analysis and control techniques for compact wide-stopband filters design," *IEEE Transactions on Circuits and Systems II: Express Briefs*, Vol. 71, No. 7, 3338–3342, 2024.

[2] Pradhan, N. C., S. Koziel, R. K. Barik, A. Pietrenko-Dabrowska, and S. S. Karthikeyan, "Miniaturized dual-band SIW-based bandpass filters using open-loop ring resonators," *Electronics*, Vol. 12, No. 18, 3974, 2023.

[3] Brown, M. D. and C. E. Saavedra, "Highly selective and compact filtering antennas using dual-mode SIW resonators," *IEEE Transactions on Antennas and Propagation*, Vol. 71, No. 5, 3928–3937, 2023.

[4] Lau, J. H., "Recent advances and trends in multiple system and heterogeneous integration with TSV interposers," *IEEE Transactions on Components, Packaging and Manufacturing Technology*, Vol. 13, No. 1, 3–25, 2023.

[5] Sadhu, B., A. Paidimarri, D. Liu, M. Yeck, C. Ozdag, Y. Tojo, W. Lee, K. X. Gu, J.-O. Plouchart, C. W. Baks, *et al.*, "A 24-30-GHz 256-element dual-polarized 5G phased array using fast on-chip beam calculators and magnetoelectric dipole antennas," *IEEE Journal of Solid-State Circuits*, Vol. 57, No. 12, 3599–

3616, 2022.

[6] Guan, X., X. Zhang, S. Yin, and Y. Liu, "Compact LTCC bandpass SIW filter with high selectivity for 5G exploiting mixed coupling," *Electromagnetics*, Vol. 41, No. 5, 344–350, 2021.

[7] Huang, L., H. Cha, and S. Zhang, "Compact wideband-folded ridge substrate-integrated waveguide filter," *IEEE Microwave and Wireless Components Letters*, Vol. 30, No. 3, 241–244, 2020.

[8] Yuan, Y., L. Zhou, L. Yang, and Y. Chen, "Design of a quadruple-mode filter using folded quarter-mode substrate integrated waveguide," in *2020 German Microwave Conference (GeMiC)*, 224–227, Cottbus, Germany, Mar. 2020.

[9] Cao, R., J.-Y. Deng, R.-M. Shang, W. Lin, and Z. Chen, "Miniaturized dual-band ridged substrate integrated waveguide cavity resonator and band-pass filters," *International Journal of RF and Microwave Computer-Aided Engineering*, Vol. 32, No. 12, e23541, 2022.

[10] Zhao, L., Y. Li, Z.-M. Chen, X.-H. Liang, J. Wang, X. Shen, and Q. Zhang, "A band-pass filter based on half-mode substrate integrated waveguide and spoof surface plasmon polaritons," *Scientific Reports*, Vol. 9, No. 1, 13429, 2019.

[11] Fan, C., X. Liu, Z. Zhu, Y. Liu, and Y. Yang, "A compact quarter-mode (QM) and eighth-mode (EM) substrate integrated waveguide (SIW) filter," in *2022 IEEE MTT-S International Microwave Workshop Series on Advanced Materials and Processes for RF and THz Applications (IMWS-AMP)*, 1–3, Guangzhou, China, Nov. 2022.

[12] Liu, P., Z. Li, M. Qin, J. Yin, and X. Qiu, "Two compact bandpass filters with controllable band based on eighth-mode substrate integrated waveguide," *IEEE Transactions on Circuits and Systems II: Express Briefs*, Vol. 71, No. 2, 932–936, 2023.

[13] Shi, Z., G. Li, Y. Song, and B. Cheng, "Compact quarter mode and eighth mode substrate integrated waveguide bandpass filters with frequency-dependent coupling," *Progress In Electromagnetics Research Letters*, Vol. 97, 51–59, 2021.

[14] Liu, L. and L. Huang, "Compact eighth-mode ridged substrate integrated waveguide filter," *Electronics Letters*, Vol. 57, No. 25, 983–985, 2021.

[15] Gu, L. and Y. Dong, "Compact half-mode SIW filter with high selectivity and improved stopband performance," *IEEE Microwave and Wireless Components Letters*, Vol. 32, No. 9, 1039–1042, 2022.

[16] Delmonte, N., M. Bozzi, L. Perregrini, and C. Tomassoni, "Cavity resonator filters in shielded quarter-mode substrate integrated waveguide technology," in *2018 IEEE MTT-S International Microwave Workshop Series on Advanced Materials and Processes for RF and THz Applications (IMWS-AMP)*, 1–3, Ann Arbor, MI, USA, Jul. 2018.

[17] Huang, X., "Design of miniaturized SIW filter loaded with improved CSRR structures," *Electronics*, Vol. 12, No. 18, 3789, 2023.

[18] Huang, L. and N. Yuan, "A compact wideband SIW bandpass filter with wide stopband and high selectivity," *Electronics*, Vol. 8, No. 4, 440, 2019.

[19] Niembro-Martín, A., V. Nasserddine, E. Pistono, H. Issa, A.-L. Franc, T.-P. Vuong, and P. Ferrari, "Slow-wave substrate integrated waveguide," *IEEE Transactions on Microwave Theory and Techniques*, Vol. 62, No. 8, 1625–1633, 2014.

[20] Nasser, M., A. R. Celik, and S. Helhel, "SIW-DGS bandpass filter design for C band satellite communications," *Sādhanā*, Vol. 48, No. 2, 55, 2023.

[21] Namanathan, P. and G. Nagarajan, "Realization of dual-mode, high-selectivity SIW cavity bandpass filter by perturbing circular shape vias," *Applied Physics A*, Vol. 128, No. 9, 773, 2022.

[22] Huang, X., X. Zhang, L. Zhou, J.-X. Xu, and J.-F. Mao, "Low-loss self-packaged Ka-band LTCC filter using artificial multimode SIW resonator," *IEEE Transactions on Circuits and Systems II: Express Briefs*, Vol. 70, No. 2, 451–455, 2022.

[23] Zhu, F., Y. Wu, P. Chu, G. Q. Luo, and K. Wu, "Compact dual-band filtering baluns using perturbed substrate integrated waveguide circular cavities," *IEEE Microwave and Wireless Technology Letters*, Vol. 33, No. 6, 663–666, 2023.

[24] Yang, X.-L., X.-W. Zhu, and X. Wang, "Dual-band substrate integrated waveguide filters based on multi-mode resonator overlapping mode control," *IEEE Transactions on Circuits and Systems II: Express Briefs*, Vol. 70, No. 6, 1971–1975, 2023.

[25] Zhu, Y. and Y. Dong, "A compact dual-band quasi-elliptic filter based on hybrid SIW and microstrip technologies," *IEEE Transactions on Circuits and Systems II: Express Briefs*, Vol. 69, No. 3, 719–723, 2021.

[26] Zheng, Y., Y. Zhu, Z. Wang, and Y. Dong, "Compact, wide stopband, shielded hybrid filter based on quarter-mode substrate integrated waveguide and microstrip line resonators," *IEEE Microwave and Wireless Components Letters*, Vol. 31, No. 3, 245–248, 2021.

[27] Lin, G. and Y. Dong, "A compact, hybrid SIW filter with controllable transmission zeros and high selectivity," *IEEE Transactions on Circuits and Systems II: Express Briefs*, Vol. 69, No. 4, 2051–2055, 2022.

[28] Jiao, M. R., F. Zhu, P. Chu, W. Yu, and G. Q. Luo, "Compact hybrid bandpass filters using substrate-integrated waveguide and stripline resonators," *IEEE Transactions on Microwave Theory and Techniques*, Vol. 72, No. 1, 391–400, 2023.

[29] Wang, X., X.-W. Zhu, Z. H. Jiang, Z.-C. Hao, Y.-W. Wu, and W. Hong, "Analysis of eighth-mode substrate-integrated waveguide cavity and flexible filter design," *IEEE Transactions on Microwave Theory and Techniques*, Vol. 67, No. 7, 2701–2712, 2019.

[30] Cameron, R. J., "Advanced coupling matrix synthesis techniques for microwave filters," *IEEE Transactions on Microwave Theory and Techniques*, Vol. 51, No. 1, 1–10, 2003.

[31] Chu, Q.-X. and H. Wang, "A compact open-loop filter with mixed electric and magnetic coupling," *IEEE Transactions on Microwave Theory and Techniques*, Vol. 56, No. 2, 431–439, 2008.

[32] Wang, F., J. Kou, X. Yin, J. Liu, K. Jing, N. Yu, Y. Yang, and Q. Li, "A compact fifth-order SIW BPF based on TSV technology with high selectivity," *Microelectronics Journal*, Vol. 144, 106067, 2024.

[33] Zheng, Y. and Y. Dong, "Miniaturized hybrid filter using stripline and LC-loaded SIW resonators," *IEEE Transactions on Circuits and Systems II: Express Briefs*, Vol. 69, No. 9, 3719–3723, 2022.

[34] Zhu, Y., Y. Dong, J. Bornemann, L. Gu, and D. F. Mamedes, "An inline compact SIW bandpass filter with quasi-elliptic response using microstrip extracted-pole resonators," *IEEE Transactions on Circuits and Systems II: Express Briefs*, Vol. 70, No. 6, 1856–1860, 2022.